Gearbox PHY for Energy-Efficient Physical Layer: Concept and Demonstration

Ahmad Nimr*, Yash Richhariya†, Zhitao Lin†, Abdo Gaber‡, Michael Löhning‡,
Vincent Kotzsch‡, and Gerhard Fettweis*
*Vodafone Chair Mobile Communication Systems, Technische Universität Dresden, Dresden, Germany
†Barkhausen Institut, Dresden, Germany
‡Emerson, NI Test and Measurement, Dresden, Germany

***Abstract*—Energy efficiency is a fundamental objective for 6G systems and requires adaptive radio operation beyond conventional modulation and coding. While existing approaches rely on duty cycling or component deactivation, substantial savings require hardware-aware adaptability, particularly under low and moderate traffic conditions. This paper investigates a practical Gearbox PHY architecture with a finite set of hardware-aware operating modes (”gears”), each defined by distinct power amplifier (PA) configurations and corresponding achievable SINR ranges. Unlike theoretical designs that assume unconstrained hardware reconfiguration, the proposed approach is compatible with 3GPP NR resource structures and standard signaling. Energy-efficient operation is formulated as a joint optimization of gear selection and discrete time-frequency resource allocation. A real-time testbed based on an OpenAirInterface gNB with dual switchable PAs and synchronized power measurements validates the concept and confirms that multi-gear operation achieves significant energy savings compared to conventional duty cycling using a single transceiver optimized for peak performance.**

***Index Terms*—Energy efficiency, Gearbox PHY, 5G NR, hardware-aware resource allocation, duty cycling.**

I. Introduction

Achieving high energy efficiency (EE) is a fundamental objective of 6G wireless networks. Industrial, academic, and standardization communities widely agree that future systems must significantly reduce energy consumption and carbon emissions while continuing to support increasing traffic volume, device diversity, and service complexity [7]. Although no explicit ITU target has been defined, improvement factors between 10x and 100x relative to 5G are frequently cited as indicative goals. Because base stationss (BSs) dominate network energy consumption, particularly within the radio access network (RAN) [9], [8], most EE efforts focus on the physical layer (PHY) and radio unit (RU) design.

A key observation is that mobile traffic is highly bursty, with long periods of low or moderate load. Nevertheless, network infrastructure is provisioned for peak demand, leading to low average resource utilization and significant energy-saving potential. Recent studies show that idle-mode signaling and availability can consume comparable or even higher energy than payload transmission during low load [9]. Consequently, 5G and 5G-Advanced introduced mechanisms such as cell sleep modes, discontinuous reception/transmission (DRX/DTX), and lean signaling [2], [10]. For 6G, energy efficiency is expected to be integrated from the first rollout [3], [4].

At the PHY level, energy-saving mechanisms include component-level shutdown, bandwidth adaptation, antenna deactivation, transmit-power control, and waveform optimization [8], [11]. For example, dynamically switching off power amplifiers (PAs) during inactive periods can yield substantial savings, while reducing spectral efficiency lowers load-dependent RU consumption. However, conventional PHY adaptation relies primarily on adaptive modulation and coding (AMC) under fixed hardware (HW) assumptions. Such approaches optimize spectral efficiency (SE) versus EE trade-offs under continuous transmission [12], but often neglect operational aspects such as duty cycling, packet-level requirements, and HW operating points. A more radical approach is the Gearbox PHY, which introduces multiple transceiver configurations (”gears”) and dynamically selects among them based on data-rate requirements [13], [14]. These works define gears by different ADC/DAC resolutions, bandwidths, or waveform options, and joint optimization of HW parameters and duty cycle minimizes energy consumption for a given effective throughput. While providing valuable theoretical bounds, such approaches assume near-continuous HW flexibility and idealized power models, which are difficult to realize in standardized systems.

This work adopts a practical and 3GPP-compliant realization of the Gearbox PHY concept. Instead of unconstrained HW reconfiguration, a finite set of implementation-feasible gears is defined using capabilities already available in 5G new radio (NR) and emerging 6G frequency bands. Each gear is characterized by a measured data-rate versus power-consumption curve that captures non-ideal HW behavior. Energy-efficient operation is formulated as a joint optimization of gear selection and discrete NR resource allocation under time-frequency constraints. Adaptation within a gear relies on standard-compliant AMC, while gear switching operates on a slower time scale aligned with traffic dynamics.

To validate the concept, a real-time end-to-end testbed based on an OpenAirInterface gNB with two switchable PAs and synchronized power measurements is developed. The framework enables experimental quantification of achievable energy gains relative to a single-architecture reference design. By bridging theoretical modeling with measurement, this work demonstrates a practical pathway toward HW-aware PHY adaptation for EE in 6G systems.

The remainder of the paper is organized as follows. Section II presents an overview of the general Gear PHY concept, followed by the 3GPP-compliant design in Section III. A concrete design example is then presented in Section IV. Section V is dedicated to the real-time testbed and measurement results. Finally, the paper is concluded in Section VI.

II. Gearbox PHY Concept and Architecture

The achievable data rate of a multiple-input, multiple-output (MIMO) system with bandwidth B, S spatial streams, and corresponding signal-to-interference-plus-noise ratios (SINRs) $\{\rho_s\}$ is given by the well-known Shannon expression

$$R_{\text{ach}} = \sum_{s=1}^{S} B \log_2(1+\rho_s). \quad (1)$$

The achievable SINR depends on several factors, including transmit power, antenna configuration, channel characteristics, HW impairments, bandwidth, noise power, and interference. Thus, achieving a target data rate requires jointly tuning the bandwidth B and per-stream SINR ρ_s under practical constraints. For example, rank-deficient channels limit the number of spatial streams S, while interference-limited conditions constrain achievable SINR, thereby restricting the attainable data rate. Within the range of achievable data rates, multiple transceiver architectures can be used to deliver a required data rate. These architectures differ in bandwidth usage, number of spatial streams, and per-stream SE, defined as

$$SE_s = \log_2(1+\rho_s). \quad (2)$$

Each architecture is associated with a distinct HW complexity and power-consumption profile. In particular, the power consumption of the analog-to-digital (ADC) scales with the sampling rate, which is proportional to the bandwidth, and the resolution, which are both closely related to SE. Moreover, the waveform and modulation choices should be adapted to the required SE. As discussed in [15], impulse modulation combined with a 1-bit ADC is most energy-efficient at very low SE (below 0.1 bit/s/Hz), while schemes such as zero crossing modulation (ZXM) are preferable at low SE (0.5 to 1 bit/s/Hz), and linear waveforms such as orthogonal frequency division multiplexing (OFDM) and its variant with quadrature amplitude modulation (QAM) become favorable at higher SE (larger than 1 bit/s/Hz). This observation highlights that no single transceiver architecture is energy-optimal across all operating regimes.

In practical operation, the required data rate R_d is typically well below the achievable data rate. Thus, resource allocation across time, frequency, power, and spatial dimensions is employed to meet the required data rate. If unused resources can be deactivated, energy savings become possible. For instance, if $R_d = \alpha R_{\text{ach}}$, where $0 < \alpha \leq 1$, the transceiver can be switched off for a fraction $(1-\alpha)$ of the time. Alternatively, fewer spatial streams can be utilized so that unused radio frequency (RF) chains can be deactivated. However, when applied to a fixed transceiver architecture, such mechanisms alone do not necessarily yield energy-optimal operation [14].

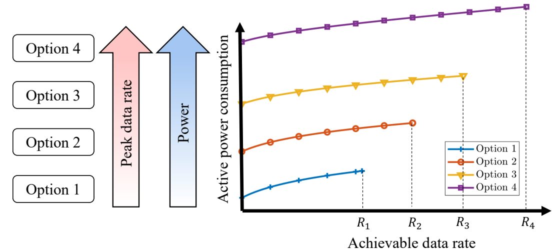

Fig. 1: The concept of gearbox PHY with multiple options

A. Gearbox PHY concept

The Gearbox PHY formalizes this idea by introducing a discrete set of PHY operating modes, referred to as gears. Each gear represents a fixed, implementation-feasible transceiver configuration characterized by a bounded achievable data rate range and a corresponding power-consumption profile, as illustrated in Fig. 1. Higher gears support higher data rates but incur higher power consumption in the fully active state. Importantly, the Gearbox PHY does not assume continuous or unconstrained HW reconfiguration. Instead, adaptation is restricted to a finite set of gears, enabling low-overhead control and compatibility with standardized PHY operation. Within a selected gear, conventional adaptation mechanisms such as AMC and power allocation are applied to meet given data rate requirements. However, reducing radiated transmit power does not necessarily translate into proportional energy savings, as the dominant direct current (DC) power consumption of RF components may remain largely unchanged. This motivates gear-level switching of HW operating points rather than fine-grained power adaptation alone.

B. Operational optimization

The Gearbox PHY operation focuses on optimizing the energy consumption of payload data transmission. Control and synchronization signaling, which are largely dictated by the standard, are assumed to be fixed and are therefore excluded from the optimization. This distinction allows the proposed framework to complement existing signaling-reduction techniques [9] by explicitly addressing the dominant energy contribution during active data transmission. For a given data packet of size N_d bits and a time constraint T_d, the required average data rate is $R_d = \frac{N_d}{T_d}$. This requirement can be met by transmitting at an achievable data rate for a fraction α of the available time, i.e., $R_d = \alpha R_{\text{ach}}$, while remaining inactive otherwise. This problem can be formulated as

$$\begin{aligned}
\min_{g} \quad \min_{\alpha^{(g)}, B_{\text{on}}^{(g)}, \{\rho_s^{(g)}\}} \quad & \alpha^{(g)} T_d P_{\text{active}}^{(g)} + \left(1-\alpha^{(g)}\right) T_d P_{\text{inactive}}^{(g)} \\
\text{s.t.} \quad & R_d = \alpha^{(g)} B_{\text{on}}^{(g)} \sum_{s=1}^{S} \log_2\left(1+\rho_s^{(g)}\right), \\
& 0 < B_{\text{on}}^{(g)} \leq B^{(g)}, 0 \leq \rho_s^{(g)} \leq \rho^{(g)}, \\
& 0 < \alpha^{(g)} \leq 1.
\end{aligned}$$

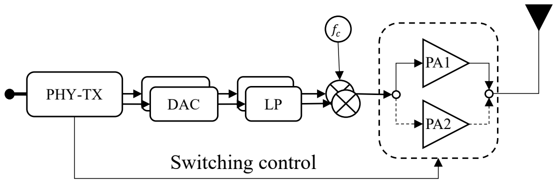

Fig. 2: Gearbox PHY with two PA options

Here, $P^{(g)}_{\text{active}}$ denotes the power consumption of the g-th gear during active transmission and may depend on the allocated power and frequency resources. $P^{(g)}_{\text{inactive}}$ represents the power consumption when no data transmission is ongoing.

The inner minimization determines the energy-optimal resource allocation within a given gear, while the outer minimization selects the most energy-efficient gear. The parameter $\rho^{(g)}$ imposes an upper bound on the achievable SINR for gear g, implicitly capturing limitations due to maximum transmit power, channel conditions, and interference. The parameter $B^{(g)}_{\text{on}}$ denotes the active bandwidth allocated within gear g, while $B^{(g)}$ represents the maximum available bandwidth. The achievable data rate within a gear depends on the frequency and power allocation across the spatial streams. When operating within standardized PHY frameworks, additional constraints arise from the set of available configuration options defined by the standard, as discussed in Section III.

C. Gearbox PHY design

A Gearbox PHY can be realized by introducing flexibility in a selected subset of HW components rather than assuming unconstrained reconfigurability. Examples include multiple PAs with different maximum output power or efficiency characteristics, as illustrated in Fig. 2, as well as multiple ADCs with different resolutions and sampling rates. Each gear corresponds to a specific transceiver configuration, whose achievable data rate and power consumption are determined by the behavior models of the selected HW components. In this sense, a transceiver with a variable number of active RF chains can be interpreted as a Gearbox PHY, where the gear index corresponds to the number of active chains.

III. 3GPP COMPLIANT GEARBOX DESIGN

5G NR, which forms the basis for the evolution toward 6G radio access, already provides a high degree of flexibility that can be exploited for the design and operation of a Gearbox PHY. In addition to emerging 6G features [11], this flexibility enables the definition of multiple operating modes without requiring explicit changes to the standard. These operating modes can be combined with multiple transceiver options, each optimized for a specific achievable data-rate range, thereby enabling the realization of the abstract Gearbox PHY concept introduced in Section II within a 3GPP framework.

Parameters such as channel bandwidth, subcarrier spacing, carrier frequency, and the number of supported MIMO streams can be used to define individual gears. In conjunction with the selected HW components for each gear, only a subset of modulation coding scheme (MCS) values may be supported. For example, when using a low-power PA together with a large bandwidth, the achievable spectral efficiency is typically limited, and the corresponding gear may only support low-order modulation and coding rates. Similarly, the maximum supported modulation order is constrained by the resolution of the digital-to-analog (DAC)/ADC. The time-frequency resource grid defined by the standard imposes additional constraints. In particular, the usable bandwidth is restricted to an integer number of physical resource blocks (PRBs), and duty cycling can only be realized at the granularity of slots. Since the standard defines a finite set of MCSs, each associated with a discrete spectral efficiency, the energy-optimization problem within a given gear can be reformulated in terms of discrete resource-allocation variables.

A. Resource allocation and gear selection

The energy-efficient operation within a gear can be expressed as the minimization of the total energy consumed over a scheduling interval by selecting the number of active slots, the number of allocated PRBs, and the spectral efficiency chosen from the standardized MCS tables. The optimization is subject to meeting the required data rate R_d, respecting the maximum available bandwidth, and ensuring that the selected spectral efficiency is supported by the achievable SINR at the resource-element level. In this formulation, the number of active slots determines the duty cycle, while the number of allocated PRBs and the selected MCS jointly determine the instantaneous transmission rate. The resource-allocation optimization for energy efficiency within a gear can be reformulated as

$$\begin{aligned} \min_{N_{\text{active}}, N_{\text{PRB}}, \text{SE}} \quad & N_{\text{active}} T_{\text{slot}} P_{\text{active}} + N_{\text{inactive}} T_{\text{slot}} P_{\text{inactive}} \\ \text{subject to} \quad & R_d \leq \frac{N_{\text{active}} N_{\text{PRB}} N_{\text{RE, data}} \text{SE}}{N_{\text{slots}} T_{\text{slot}}}, \\ & N_{\text{active}} + N_{\text{inactive}} = N_{\text{slots}} \\ & N_{\text{PRB}} \leq N_{\text{PRB,max}}, \; 1 \leq N_{\text{active}} \leq N_{\text{slots}}, \\ & \text{SE} \in \text{ MCS table}, \\ & \text{SE} \leq \log_2(1 + \text{SINR}_{\text{max}}). \end{aligned} \tag{3}$$

Here, N_{active} is the number of active slots, each of duration T_{slot}, and thus determines the fraction of time during which the transmitter is active, while N_{slots} corresponds to the transmission periodicity. The number of allocated PRBs per slot, N_{PRB}, determines the occupied bandwidth, where $N_{\text{PRB,max}}$ denotes the maximum number of available PRBs. Each PRB contains a fixed number of data-bearing resource elements (REs) $N_{\text{RE, data}}$. The selected SE is constrained by the maximum achievable SINR, denoted by SINR_{max}, which is bounded by the capabilities of the selected gear and its underlying hardware and resource configuration. In this formulation, both SINR and SE are defined at the RE level.

The optimization problem needs to be solved for each gear, and then the gear that achieves the minimum energy consumption is selected. Since all optimization variables take values from finite discrete sets, the problem can be solved via exhaustive search. Specifically, the energy consumption is

TABLE I: Resource configuration according to 3GPP TS 38.214 [16]

Frequency (TTD mode)	3.3197 GHz
Channel bandwidth	40 MHz
Subcarrier spacing	30 KHz
Slot duration	$T_{\text{slot}} = 0.5$ ms
# Available PRBs	$N_{\text{PRB, max}} = 106$
# Subcarriers per PRB	12
# PDSCH OFDM symbols per slot	13
# DMRS RE per PRB	12
# Data bearing REs per PRB	$N_{\text{RE, data}} = 144$
# Active subcarriers	$K = 1272$
# FFT size	$N = 2048$
# Slots (N_{slots}) per half frame	10 (7DL,1S,2UL)
MCS table	Table 5.1.3.1-2

evaluated for all feasible combinations of N_{active}, N_{PRB}, and SE that satisfy the constraints, and the configuration yielding the minimum energy consumption is selected.

B. Operation modes

The Gearbox PHY supports two modes of operation: a real-time mode and a longer-term adaptation mode. The two operation modes naturally align with different 3GPP time scales: a fast, slot-level mode compatible with MAC/PHY scheduling, and a slower, semi-static mode governed by higher-layer configuration. In the first mode, gear switching is performed in real time without imposing significant reconfiguration of the BS, such as changes to carrier configuration or bandwidth parts (BWPs). This mode relies on controlling flexible HW components and can be transparently integrated into the resource-allocation procedure. For example, the achievable SINR and the corresponding energy cost can be estimated for each gear, and the transmitter selects the gear that minimizes energy consumption. Specifically, in a design based on multiple PAs, as illustrated in Fig. 2, the appropriate PA is activated prior to transmission. In this case, no additional signaling beyond existing downlink control information (DCI) is required. For receiver-side gearbox designs based on ADC reconfiguration, the receiver can infer the appropriate gear from the MCS information conveyed in the DCI. The second mode of operation involves reconfiguration of radio resources, such as carrier frequency, bandwidth, subcarrier spacing, and supported MIMO layers, which affect both coverage and scheduling. This mode is particularly suitable for adapting the Gearbox PHY to longer-term variations, such as traffic load, mobility patterns, or service-level requirements, and can be configured via semi-static or radio resource control (RRC) procedures. For instance, when the expected traffic load is low, the BS can be reconfigured with smaller bandwidth.

IV. Design Example

This section presents a simplified Gearbox PHY design example with two PAs, as illustrated in Fig. 2, operating in a flat-fading line of sight (LoS) channel. Experimental evaluation and measurements are provided in Section V. The underlying resource configuration is summarized in Table I. To simplify the analysis, the full available bandwidth is utilized, i.e., $N_{\text{PRB}} = N_{\text{PRB, max}}$. Consequently, the optimization problem in (3) reduces to determining the number of active slots and the selected SE. Each gear is associated with a maximum achievable SINR, which depends on the maximum output power and characteristics of the corresponding PA. The higher gear achieves a larger SINR at the cost of increased power consumption.

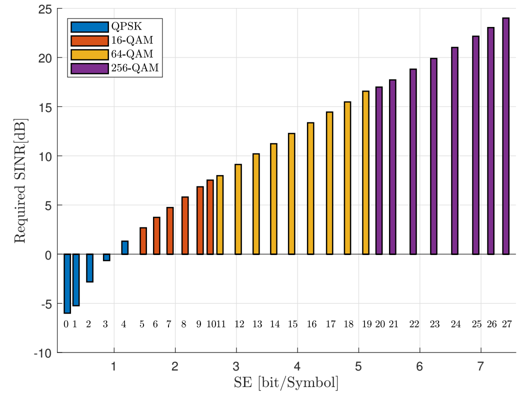

Fig. 3: SINR requirements for SE defined in 3GPP TS 38.214 MCS Table 5.1.3.1-2

A. SINR requirements

To determine the feasible SE values, it is necessary to map the SE values from the MCS table to their corresponding SINR requirements. The theoretical achievable rate can be derived from the additive white Gaussian noise (AWGN) model $y = d+v$, which represents the equivalent signal model after equalization. Here, d is uniformly distributed M-QAM symbol selected from the constellation $\mathcal{C}_M = \{d_1, \cdots, d_M\}$ with variance $\mathrm{E}\left[|d|^2\right] = 1$ and v is AWGN with variance $\mathrm{E}\left[|v|^2\right] = 1/\rho$, where ρ denotes the SINR. The mutual information [bit/symbol] is given by

$$I(M,\rho) = \frac{\log_2(e)}{M} \int_y \sum_{m=1}^{M} f(y|d_m) \log\left(\frac{f(y|d_m)}{f(y)}\right) dy, \quad (4)$$

where the distributions are given by $p(d_m) = \frac{1}{M}$, $f(y|d_m) = \frac{\rho}{\pi} e^{-\rho|y-d_m|^2}$, and $f(y) = \frac{1}{M}\sum_{m=1}^{M} f(y|d_m)$. The resulting theoretical SINR corresponding to the SE values defined in 3GPP MCS Table 5.1.3.1-2 are illustrated in Fig. 3. In practice, additional implementation loss should be considered, accounting for channel estimation and equalization errors, and for inaccurate estimation of the SINR.

B. Achievable SINR in flat channel

Considering a flat-fading LoS channel, the achievable SINR per allocated RE can be expressed as

$$\rho = \frac{G_L G_{\text{PA,eff}} G_\phi}{G_L \sigma_z^2 + \sigma_v^2 + \sigma_q^2 + \sigma_\phi^2} \frac{N}{K} P_s, \quad (5)$$

This document is a preprint of: A. Nimr, Y. Richhariya, Z. Lin et al., “Gearbox PHY for Energy-Efficient Physical Layer: Concept and Demonstration,” in Proceedings of 2026 Joint European Conference on Networks and Communications & 6G Summit (EuCNC/6G Summit 2026), Malaga, Spain, Jun 2026.

where P_s corresponds to the signal power at the input of the PA, i.e., $P_s = \mathrm{E}\left[|s(t)|^2\right]$. The transmitted signal at the output of PA is then given by

$$s^{(\mathrm{tx})}(t) = \sqrt{G_{\mathrm{PA,eff}}}s(t) + z(t), \tag{6}$$

where, $G_{\mathrm{PA,eff}}$ is the effective PA power gain, and $z(t)$ represents the PA nonlinear distortion. Following the Bussgang decomposition, this distortion can be approximated as an additive uncorrelated noise term with variance σ_z^2, which depends on the input signal peak-to-average power ratio (PAPR) and applied output back-off. G_L denotes the path gain, $\sigma_v^2 = BF_{\mathrm{LNA}}N_0$ is the total noise power, accounting for bandwidth B, thermal noise power density N_0, and low noise amplifier (LNA) noise figure F_{LNA} in linear scale. The term σ_q^2 denotes the quantization noise, which depends on the automatic gain control (AGC) configuration. σ_ϕ^2 models additive interference corresponding to the phase noise, while G_ϕ represents the common phase error (CPE) gain. The parameters N and K denote the discrete Fourier transform (DFT) size and number of active resource elements, respectively. In this design example, the gears are identical except for the selected PAs. Therefore, the SINR difference arises primarily for the gain $G_{\mathrm{PA,eff}}$ and the distortion variance σ_z^2, which depends on the modulation order associated with the selected SE. The achievable SINR for each gear serves as an input to the optimization problem.

C. Impact of channel estimation and equalization

The received signal after DFT processing is expressed as $\tilde{y}[k] = hd_k + \tilde{w}[k]$, where $\tilde{w}[k]$ aggregates thermal noise and effective additive distortion terms (PA nonlinearity, quantization, phase-noise-induced interference), which are approximated as uncorrelated with the data symbols. Assuming uncorrelated data symbols with $\mathrm{E}\left[|d_k|^2\right] = 1$, the ideal SINR is given by $\rho = |h|^2/\sigma_w^2$. The channel is estimated from pilot symbols from the samples $\tilde{y}[p] = hd_p + \tilde{w}[p]$. Using, P pilots with $d_p = 1$ the estimated channel is

$$\hat{h} = h + \frac{1}{P}\sum_{p=1}^{P}\tilde{w}[p] = h + e_h, \tag{7}$$

with estimation error $\mathrm{E}\left[|e_h|^2\right] = \frac{\sigma_w^2}{P}$. After equalization, the detected data symbols are

$$\hat{d}_k = \frac{\tilde{y}[k]}{\hat{h}} = d_k + \frac{\tilde{w}[k] - e_h d_k}{h + e_h}. \tag{8}$$

As a result, the effective post-equalization SINR depends on the channel estimation accuracy and degrades as the estimation error variance increases. The SINR can be estimated from reference symbols, such as those one used for channel estimation. Using P reference symbols, the received signal power is estimated as

$$\hat{P}_y = \frac{1}{P}\sum_{p=1}^{P}|\tilde{y}[p]|^2 \approx |h|^2 + \sigma_w^2. \tag{9}$$

Moreover, the noise variance σ_w^2 can be estimated from non-allocated RE, where $\tilde{y}[m] = \tilde{w}[m]$, using M samples,

$$\hat{\sigma}_w^2 = \frac{1}{M}\sum_{m=1}^{M}|\tilde{y}[m]|^2 \approx \sigma_w^2. \tag{10}$$

The estimated SINR is then obtained as

$$\hat{\rho} = \frac{\hat{P}_y - \hat{\sigma}_w^2}{\hat{\sigma}_w^2}. \tag{11}$$

Since σ_w^2 includes the distortion of PA non-linearity, the estimated SINR depends on the selected gear and resource allocation and may vary across OFDM symbols.

V. Experiment and Demonstration

A. Demonstration Setup

To evaluate the proposed Gearbox design, a real-time testbed is developed as illustrated in Fig. 4, comprising a software-defined, open, and modifiable sixth generation (6G) BS (gNB) prototype with a pair of switchable PAs, a 5G user equipment (UE), and a synchronized power-measurement framework.

1) Link setup: A downlink (DL) transmission from the next generation node B (gNB) to the UE is considered. Both the gNB prototype and the UE RF front-ends are realized using *NI Ettus USRP X410* software-defined radios (SDRs) [17], interfaced with high-performance Linux servers running real-time open-source fifth generation (5G) software stacks based on OpenAirInterface (OAI) [18]. The output of the gNB transmitter is connected to an RF network consisting of two switchable PAs, which can be controlled in real time from the gNB software stack via the high-speed general purpuse input/output (GPIO) lines of the USRP. The OAI gNB stack is operated in PHY test mode, which provides increased flexibility in configuring the multiple access control (MAC) layer. This enables synchronized switching of the PAs at slot boundaries of the 5G NR downlink transmission. The first PA (PA_1), used in the lower gear, is the energy-efficient *SKY67154-396EK1*, featuring a reduced gain (typical small-signal gain of 19 dB at 2500 MHz) and lower power consumption (approximately 0.35 W). The second PA (PA_2), used in the higher gear, is the higher-gain *Mini-Circuits ZRON-8G+* amplifier, providing up to 24.5 dB gain, with higher power consumption.

2) Power measurement framework: To holistically measure and evaluate the obtained energy savings, a measurement framework is developed that can continuously and synchronously measure the power consumption of multiple heterogeneous components of a wireless system under test, namely the gNB prototype. The power measurement framework consists of two main components: (i) a scalable NI CompactRIO (cRIO) measurement system [19], and (ii) a central test orchestration and data recording entity that runs on a third Linux server. The NI cRIO measurement system comprises *NI-9244* and *NI-9238* modules for measuring AC voltages and currents and *NI-9229* and *NI-9227* modules for

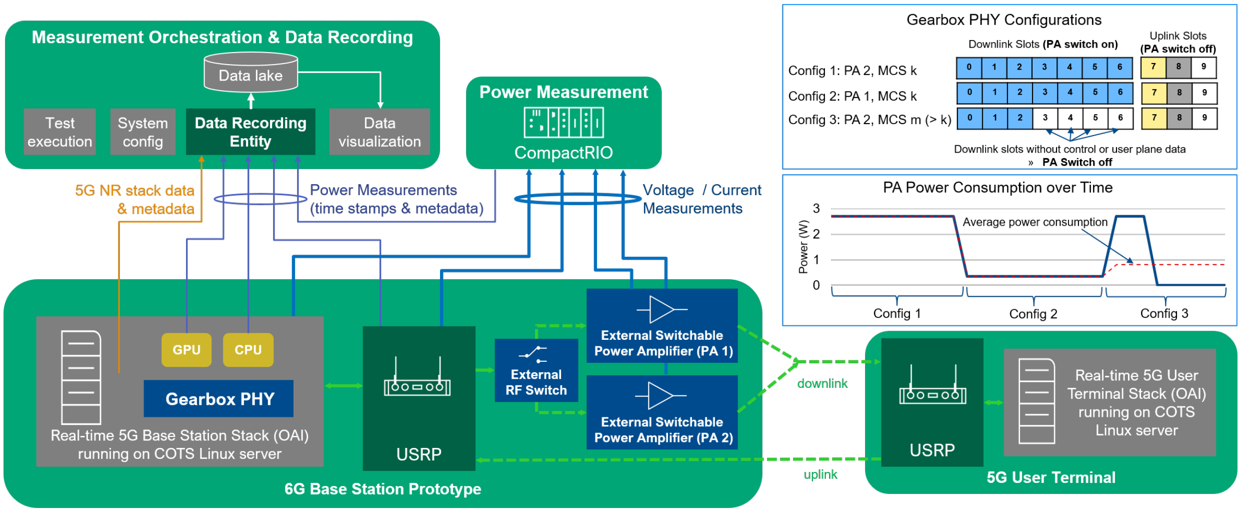

Fig. 4: Block diagram of Gearbox PHY real-time testbed with example Gearbox PHY configurations

measuring DC voltages and currents. All cRIO modules are installed in the *NI cRIO-9047* controller for running power calculations and data aggregation. The cRIO system measures the alternating current (AC) voltage and current at the power supplies of the gNB server and the USRP, as well as DC voltage and current at the power supplies of the switchable PAs. It derives the respective instantaneous component power consumption over time.

The central data recording entity receives all power measurements from the cRIO system and can receive further measurements from embedded CPU and GPU power sensors in the base station server and power sensors in the gNB USRP. In addition, data and configuration parameters can be transferred from the base station stack. The latter can act as metadata for the respective power measurements to e.g., enable advanced data analytics. By using timestamps and metadata like slot identifier (ID) and frame ID, the data recording entity synchronizes all measurements from the different sensors and sources to a common time grid. In the studied case, the 500 μs slot grid of the 5G NR system. The synchronized measurements are finally stored as JavaScript object notation (JSON) or Signal Metadata Format (SigMF) [20] files to a data lake from where they can be read out for further analysis and visualization.

B. Experiment Scenario

1) Evaluation of PA performance: The first experiment investigates the performance of both PAs across different MCS and noise levels. The power of the transmitted signal $S(t)$ at the output of the gNB SDR is set to $P_s = -9.7$ dBm. The channel gain is set to $G_L = -38$ dB, which is implemented via attenuation. The measured signal power of the received signal, $r^{(\mathrm{rx})}(t) = G_L s^{(\mathrm{tx})}(t)$, at the input of UE is given by

$$P_{\mathrm{rx}} = G_L G_{\mathrm{PA,eff}} P_s \left(1 + \frac{\sigma_z^2}{P_s G_{\mathrm{PA,eff}}}\right). \tag{12}$$

Using a spectrum analyzer, the measured received powers for PA_1 is $P_{\mathrm{rx},1} = -33.6$ dBm, and for PA_2 $P_{\mathrm{rx},2} = -26.4$ dBm. These values remain approximately constant across different modulation orders. This is expected, since the PAPR of OFDM is largely independent of the modulation order.

To estimate the actual PA gain, the hardware-limited region, where distortion dominates thermal noise is used. The estimated SINR can be approximated as

$$\rho_{\mathrm{I}} \approx \frac{G_{\mathrm{PA,eff}}}{\sigma_z^2}\frac{N}{K}P_s, \Rightarrow \frac{\sigma_z^2}{G_{\mathrm{PA,eff}}} = \frac{N}{K}\frac{P_s}{\rho_I}, \tag{13}$$

assuming $|G_\phi| \approx 1$ and that PA distortion is the dominant impairment. This allows estimation of the effective gain and distortion variance, such that

$$G_{\mathrm{PA,eff}} = \frac{P_{\mathrm{rx}}}{G_L P_s \left[1 + \frac{N}{K}\frac{P_s}{\rho_I}\right]}, \quad \sigma_z^2 = \frac{P_{\mathrm{rx}}}{G_L} - G_{\mathrm{PA,eff}} P_s. \tag{14}$$

The estimated gain and distortion levels for different MCS are listed in Table II. The results confirm that the modulation order has negligible impact on the effective gain. Moreover, PA_2 provides approximately 7.1 dB higher gain than PA_1, but introduces approximately 7.7 dB higher distortion.

In the noise-limited region, where thermal noise dominates hardware distortion, the SINR can be approximated as

$$\rho_N \approx \frac{G_L G_{\mathrm{PA,eff}}}{\sigma_v^2}\frac{N}{K}P_s. \tag{15}$$

To emulate different SINR levels, additional AWGN is injected using a calibrated noise generator based on GNU Radio Fast Noise Source [21] and NI Ettus USRP B210 SDR [22]. The generator is initially configured to $\sigma_v^2 = -58$ dBm, ensuring that thermal noise exceeds $G_L \sigma_z^2$ by more than 10 dB. The measured performance of both PAs is evaluated relative to a reference signal-to-noise ratio (SNR) obtained without PAs, defined as $\rho_0 = \frac{G_L}{\sigma_v^2}\frac{N}{K}P_s$. The results are shown in Fig. 5. The reference SNR can be used as a decision metric to select the appropriate PA.

These measurements confirm the approximately 7 dB gain advantage of PA_2. The effective SINR is shifted by the PA

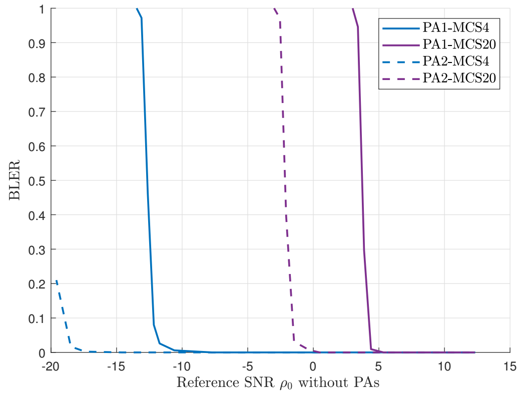

Fig. 5: Measured performance of PAs relative to reference SNRs estimated prior to PAs gain

TABLE II: Estimated PA gain and interference

	QPSK	64-QAM	256-QAM
$\mathrm{PA}_1:\ \rho_I$ [dB]	42.31	42.08	41.71
$\mathrm{PA}_1:\ G_{\mathrm{PA,eff}}$ [dB]	14.1	14.1	14.1
$\mathrm{PA}_1:\ \sigma_z^2$ [dBm]	-45.54	-45.31	-44.94
$\mathrm{PA}_2:\ \rho_I$ [dB]	41.65	41.41	41.35
$\mathrm{PA}_2:\ G_{\mathrm{PA,eff}}$ [dB]	21.2	21.2	21.2
$\mathrm{PA}_2:\ \sigma_z^2$ [dBm]	-37.78	-37.54	-37.48

gain. For example, for PA_2 (effective gain = 21.1 dB), the required SINR to achieve 10% block error rate (BLER) at MCS4 is approximately 3 dB. This value is slightly higher than the theoretical SINR in Fig. 3, which is expected due to practical implementation losses such as channel estimation inaccuracies and decoding losses.

2) Energy savings demonstration: In the second experiment, the EE trade-offs is evaluated when using duty-cycled operation of the high-performance PA_2, at higher MCS indices to achieve throughput equivalent to continuous operation of PA_1 at lower MCS levels. The analysis quantifies whether burst transmission at higher data rates with intermittent PA operation can yield net energy savings compared to continuous transmission at lower rates. For a reference SNR $\rho_0 = 0$ dB, it can be seen from Fig. 5, that PA_1 can only operate in lower MCS, whereas PA_2 can achieve higher data rate with MCS 20. Fig. 6 shows the achievable rate for both PA and the corresponding power consumption when fully active and relying on reduced input signal power P_s. It is observed that for the used PAs, the DC power consumption is constant regardless of the input power. Thus, to save energy, duty cycling is needed by switching off the unused PA. However, this experiment demonstrates that using only the high-gain PA_2 with duty cycling does not lead to best energy savings.

The experimental approach establishes throughput-equivalent operating points by matching the average data-rates between three operational configurations: (i) Config. 1 (Baseline): Continuous transmission using PA_2 at MCS k with throughput R_k, (ii) Config. 2 (Energy Efficient): Continuous transmission using PA_1 at MCS k

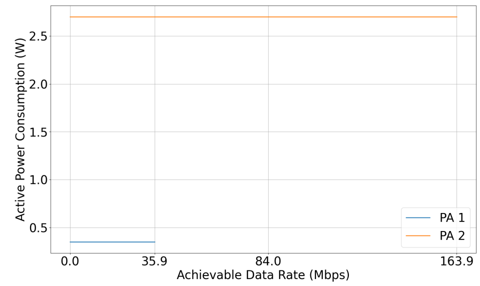

Fig. 6: Power consumption vs rate for 2-option Gearbox PHY

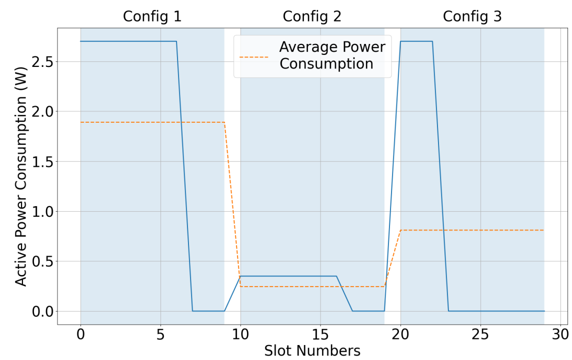

Fig. 7: Power consumption of various configurations

with throughput R_k, and (iii) Config. 3 (Duty-cycled): Burst transmission using PA_2 at MCS $m (m > k)$ with duty cycle D, achieving average throughput $R_m = R_k$. Fig. 7 illustrates the active power consumption across three equivalent average throughput considering the aforementioned configurations. The measurements are organized into 3 periods of 10 slots each, where the first 7 slots are used for DL. Config. 1 exhibits constant active power consumption of $2.7\,\mathrm{W}$ using PA_2 at MCS 4 during the 7 DL slots before dropping to zero for the remaining slots, yielding an average power consumption of $1.9\,\mathrm{W}$ across the period. Config. 2 leads to an average power consumption of $0.25\,\mathrm{W}$ using PA_1 at MCS 4. Config. 3 shows burst transmission with PA_2 at MCS 10 with peak power of $2.7\,\mathrm{W}$ during the initial 3 DL slots followed by no transmission for the next 4 DL slots, resulting in an average power consumption of $0.8\,\mathrm{W}$.

Comparatively, Config. 2, which uses PA_1, is the most energy efficient with an average power consumption of $(0.25\,\mathrm{W})$, which is 87% less than Config. 1 $(1.9\,\mathrm{W})$, and 69% less than Config. 3 $(0.8\,\mathrm{W})$. These findings establish the need for multiple PAs depending on the throughput requirement and demonstrate the trade-offs in EE between duty-cycled high-power burst transmission and continuous low-power transmission under throughput-equivalent circumstances.

VI. Conclusion

This work presented a practical realization of the Gearbox PHY concept for energy-efficient wireless communication systems. In contrast to purely theoretical hardware-flexible designs, the proposed architecture restricts adaptation to a finite set of implementation-feasible operating modes while maintaining full 3GPP compatibility. The Gearbox PHY framework was developed from theory to practice by incorporating realistic SINR modeling under hardware impairments and explicitly accounting for channel and SINR estimation effects. The abstract energy-minimization formulation was mapped onto discrete NR resource-allocation variables, enabling joint optimization of active slots, modulation and coding selection, and gear choice. A real-time experimental testbed with dual switchable PAs and synchronized power measurements validated the proposed approach. The measurements revealed distinct hardware-limited and noise-limited operating regimes and confirmed that the higher-gain PA provides a significant SINR shift at the expense of increased distortion and power consumption. The results demonstrate that dynamic gear selection enables adaptive shifting of the effective SINR operating range while minimizing total energy consumption for a given data rate requirement.

The presented Gearbox PHY framework provides insights into a practical pathway for enhancing PHY energy efficiency through multiple hardware options. This requires jointly optimizing the hardware configuration, modulation, and resource allocation to fulfill data rate and latency requirements with minimum energy consumption. While this work focuses on a simple single-user scenario to explore the potential of Gearbox PHY, the concept can be extended to more complex settings by incorporating additional constraints into the optimization. Future work will address multi-user scheduling, operation in fading channels, and long-term adaptation to traffic patterns and network load.

REFERENCES

[1] Nokia Bell Labs, “Energy efficiency in next-generation mobile networks,” Nokia, White Paper, 2023. [Online]. Available: https://www.nokia.com/asset/212810/

[2] ——, “The path to 6G with unparalleled energy savings: A 3GPP standardization perspective,” Nokia, White Paper, 2024. [Online]. Available: https://www.nokia.com/asset/214113/

[3] Samsung, “Energy Saving for 6G Network: Part II, From Always-ON to Smart-ON,” Blog post, July 2025, accessed: 2026-02-05. [Online]. Available: https://research.samsung.com/blog/Energy-Saving-for-6G-Network-Part-II-From-Always-ON-to-Smart-ON

[4] 3GPP, “Revised SID: Study on 6G Radio,” 3rd Generation Partnership Project (3GPP), 3GPP TSG RAN #110 meeting contribution RP-253876, December 2025. [Online]. Available: https://www.3gpp.org/ftp/tsg_ran/TSG_RAN/TSGR_110/Docs/RP-253876.zip

[5] Fraunhofer IIS, “6G Energy Efficiency and Sustainability,” Fraunhofer Institute for Integrated Circuits IIS, White Paper, 2023. [Online]. Available: https://www.iis.fraunhofer.de

[6] M. G. Becker, R. Krï¿½mer, M. Gunia, and F. Ellinger, “Fast-Switchable 3.6 GHz GaN Doherty Power Amplifier for Energy-Efficient Non-Continuous Transmission of 256-QAM Signals,” in *2025 IEEE/MTT-S International Microwave Symposium - IMS 2025*, 2025, pp. 1095–1098.

[7] 6G Infrastructure Association, “European Vision for the 6G Network Ecosystem,” 6G-IA, White Paper, 2024. [Online]. Available: https://6g-ia.eu/

[8] N. Alliance, “Green Future Networks: A Roadmap to Energy Efficient Mobile Networks,” *NGMN White Paper, June*, 2024.

[9] Ericsson Research, “Energy Performance of 6G Radio Access Networks,” Ericsson, White Paper, 2023. [Online]. Available: https://www.ericsson.com/en/reports-and-papers/white-papers

[10] B. Banerjee *et al.*, “6G PHY: Insights From 6G-ANNA Research Initiative,” *IEEE Open Journal of the Communications Society*, pp. 1–1, 2026.

[11] Nokia Bell Labs, “Physical Layer Foundations Powering 6G,” Nokia, White Paper, 2023. [Online]. Available: https://www.nokia.com/asset/214991/

[12] S. Han, T. Xie, and C.-L. I, “Greener Physical Layer Technologies for 6G Mobile Communications,” *IEEE Communications Magazine*, vol. 59, no. 4, pp. 68–74, 2021.

[13] F. Gast, M. Dörpinghaus, P. Sen, A. Nimr, and G. P. Fettweis, “Hardware-Aware Energy Efficiency Optimization in Wireless Communications Using a Gearbox-PHY,” *IEEE Communications Letters*, vol. 28, no. 7, pp. 1584–1588, 2024.

[14] F. Gast, F. Roth, M. Dörpinghaus, P. Sen, S. Zeitz, and G. P. Fettweis, “Energy Optimization using Joint Modulation Scheme and Front End Adaptation -the Gearbox-PHY,” in *2024 19th International Symposium on Wireless Communication Systems (ISWCS)*, 2024, pp. 1–6.

[15] G. P. Fettweis and H. Boche, “6G: The Personal Tactile Internet-And Open Questions for Information Theory,” *IEEE BITS the Information Theory Magazine*, vol. 1, no. 1, pp. 71–82, 2021.

[16] 3GPP, “NR; Physical layer procedures for data,” 3rd Generation Partnership Project (3GPP), Technical Specification TS 38.214, 2022. [Online]. Available: https://www.3gpp.org/ftp/Specs/archive/38_series/38.214/

[17] Emerson, NI Test and Measurement. (2026) USRP X4xx series (USRP X410). Online manual. [Online]. Available: https://files.ettus.com/manual/page_usrp_x4xx.html

[18] N. Nikaein, M. K. Marina, S. Manickam, A. Dawson, R. Knopp, and C. Bonnet, “OpenAirInterface: A Flexible Platform for 5G Research,” *Comput. Commun. Rev.*, vol. 44, pp. 33–38, 2014.

[19] Emerson, NI Test and Measurement. (2026) CompactRIO Systems (cRIO). [Online]. Available: https://www.ni.com/en/shop/compactrio.html

[20] The GNU Radio Foundation, Inc., “The Signal Metadata Format (SigMF),” https://sigmf.org, May 2025, released 2025-05-16. [Online]. Available: https://sigmf.org

[21] GNU Radio Community. (2025) GNU Radio Fast Noise Source. Online manual. [Online]. Available: https://wiki.gnuradio.org/index.php/Fast_Noise_Source

[22] Emerson, NI Test and Measurement. (2026) USRP B2x0 Series (USRP B210). Online manual. [Online]. Available: https://files.ettus.com/manual/page_usrp_b200.html